Journal of Power Sources 190 (2009) 141–148

Contents lists available at ScienceDirect

Journal of Power Sources

journal homepage: www.elsevier.com/locate/jpowsour

Lithium intercalation and interfacial kinetics of composite anodes formed by oxidized graphite and copper

M. Mancini[a,*], F. Nobili[a], S. Dsoke[a], F. D'Amico[b], R. Tossici[a], F. Croce[c], R. Marassi[a]

[a] Dipartimento di Scienze Chimiche, Università di Camerino, Via S. Agostino, 1, 62032 Camerino (MC), Italy
[b] Dipartimento di Fisica, Università di Camerino, Via Madonna delle Carceri, 9, 62032 Camerino (MC), Italy
[c] Dipartimento di Scienze del Farmaco, Università degli Studi "G. D'Annunzio", Via dei Vestini, 31, 66013 Chieti, Italy

ARTICLE INFO

Article history:
Received 20 August 2008
Received in revised form 8 October 2008
Accepted 14 October 2008
Available online 5 November 2008

Keywords:
Graphite anodes
Partially oxidized graphite
Cu composites

ABSTRACT

The electrochemical behavior of composite anodes prepared either by mixing partially oxidized graphite and Cu powders or by coating the pristine partially oxidized graphite electrodes with few-nanometer-thick Cu layers has been studied by slow-scan-rate cyclic voltammetry (SSCV) and galvanostatic charge/discharge cycles over the temperature range of −30 °C to 20 °C. The interfacial intercalation/deintercalation kinetics has also been investigated using electrochemical impedance spectroscopy (EIS).

The role of the Cu in improving low-temperature performances and kinetics of graphite electrodes is discussed.

1. Introduction

Graphite is the most used anodic material in lithium-ion batteries since their introduction into the market. The problem of the poor performances of graphite anodes at low temperatures is, however, still open [1–3]. While lithium deintercalation [4] is not affected by the temperature, severe polarization occurs at low temperature during intercalation. The high polarization forces the electrode to reach the deposition potential of metallic lithium (i.e. the cathodic cut off potential) before appreciable lithium loading can take place. This means that a real cell may be fully discharged but not recharged at low temperature.

The reasons of this behavior are still under debate. Ohmic, activation or concentration polarization, the decrease of the solvent conductivity, the resistance of the passivation layer or of the bulk electrode, together with the increase of charge transfer resistance at electrode/electrolyte interface and the decrease of the solid-state lithium diffusion rate, are among the possible causes.

Several means for reducing the factors affecting the polarization and thus increasing the low-temperature performances of graphite anode systems have been proposed in recent times. Mild oxidation has been demonstrated to be effective [5–7] to this purpose as it introduces surface modifications that: (i) remove surface hydroxyl groups and water; (ii) remove structural defects and hybridized sp^3 carbon atoms; (iii) create nanovoids and nanochannels that can accommodate extra Li^+ ions (at least in the first few cycles); (iv) introduce surface acidic groups and oxides that contribute to build up a pre-formed chemically bonded passivation layer which protects the active graphite particles from solvent co-intercalation [8]. Some authors have proposed modifications of the solvent/electrolyte/passivation layer system, in order to improve the transport properties of Li^+ ions and modify the active surface for charge transfer reaction [9–12]. Another route commonly investigated involves the modification of electrode formulation by addition of some finely dispersed metal powders or covering the graphite surface with a thin metal layer, in order to: (i) improve bulk conductivity of electrodes, (ii) enhance kinetics of charge transfer process, (iii) induce specific lithium–metals alloying reactions to increase reversible capacity [13–24]. In this contest it has been demonstrated that metal/graphite composite electrodes [4], obtained by mixing nanosize powders (markedly Cu, Sn and Al, approximately 1% w/o) to oxidized graphite, retain substantial intercalation ability at low temperature. At temperatures below −20 °C the thermally oxidized graphite pristine electrode does not accommodate any relevant amount of lithium while the electrodes containing metal powders still retain a relatively high intercalation capacity (up to 30% of theoretical for electrodes containing Cu, Sn and Al powders). In a recent paper [25] it has also been shown that the charge transfer resistance of electrodes covered by thin metal layers (50 Å) of Cu and Sn is considerably lower than that of unmodified electrodes. Tentatively this effect has been attributed to a direct involvement of metals in enhancing the Li^+ ion desolvation

* Corresponding author. Tel.: +39 0737 402259; fax: +39 0737 402296.
E-mail address: marilena.mancini@unicam.it (M. Mancini).

0378-7753/$ – see front matter © 2008 Elsevier B.V. All rights reserved.
doi:10.1016/j.jpowsour.2008.10.084

that is known to be the rate-determining step of the overall charge transfer process taking place at electrode/electrolyte interface [26–31].

With the purpose to further test this hypothesis, the present paper deals with the characterization of the structure, morphology and electrochemical behavior of several kinds of Cu/oxidized graphite composites, prepared by dispersing nanosize metal particles and/or applying Cu surface coatings on the pristine electrodes. The polarization phenomena and their dependence on temperature have been investigated using ac-impedance.

2. Experimental

The electrodes were prepared according to a well-established procedure reported elsewhere [4,25]. In brief, Timrex KS-15 graphite (Timcall, specific area 12 $m^2\,g^{-1}$, average particle size 7.7 μm, and interlayer distance 3.36 Å) was partially oxidized in air at 750 °C for 45 min. Before thermal treatment, the graphite samples were dried under vacuum overnight at 200 °C. The oxidation degree was roughly estimated by the weight loss (about 30%). The oxygen content (about 11%) was determined by elemental analysis [4]. The pristine electrodes, designated sample A and used for comparison purposes, were prepared using the "doctor blade" technique to coat a Cu foil current collector (12.5 μm, Schlenk) with a slurry of oxidized graphite, carbon (Super-P MMM carbon), PVdF (Aldrich) and oxalic acid (Carlo Erba) in NM2P (N-methyl-2-pyrrolidinone, Aldrich) with the following composition: graphite/carbon/PVdF/$H_2C_2O_4$ 84.5/5/10/0.5 w/o. The oxalic acid in the slurry removes surface oxides and partially etches the copper current collector improving the adhesion of the active material [4]. The unreacted acid readily decomposes or evaporates during the electrodes drying step. Nanosize-activated Cu metal powder (Aldrich ~100 nm) was used as additive to prepare the metal modified electrodes. A known amount of the metal suspension in hexane was mechanically dispersed in Super-P carbon by stirring the mixture for 12 h in a closed container using a magnetic stirrer. This dispersion was used instead of pure Super-P to prepare the slurry as previously described. The operation was performed in a dry-box with moisture and oxygen level below 5 ppm. Based on the composition of the Super-P metal dispersion, the metal content in the final electrode was about 1% w/o. In the following this type of electrodes are designated as type B. Two other types of electrodes were also prepared: electrodes C and D where type A and type B electrodes have been respectively coated with a 50 Å thick evaporated Cu layer. The metallic coatings were prepared by PVD (physical vapor deposition) in a vacuum chamber, using tungsten crucibles to hold the pure Cu metal. The metal was allowed to evaporate onto the carbon surface, kept at room temperature, by applying suitable currents to the crucible. Deposit thickness was controlled by monitoring the weight of electrodes with a quartz crystal microbalance. The experimental conditions were adjusted in order to obtain layers with a thickness of 50 Å. The graphite loading of the electrodes, either pristine or composite, was of the order of 1.5–2 mg cm^{-2}.

All the electrochemical measurements were performed using T-shaped polypropylene Swagelok type cells equipped with stainless steel (SS304) current collectors.

Two polypropylene films (Celgard 2400, Celanese Co.) were used as separators. The electrolyte was a 1 M solution of $LiPF_6$ in EC:DEC:DMC 1:1:1 (LP71, Merck). The ternary electrolyte was used in order to avoid complications due to solvent freezing and poor Li^+ ion conductivity at low temperatures [32,33]. A disk of high-purity lithium foil (Foote Mineral Co.) was used as counter electrode; a lithium strip supported on a stainless steel grid and placed between counter and working electrode was used as reference electrode. In this way, the reference electrode was placed directly in the electric field between working and counter electrodes. This arrangement helps in improving the quality of impedance measurements at low frequencies and low temperatures.

The cells were assembled in the dry-box and then cycled three times at C/3 rate in order to form a homogeneous solid electrolyte interface (SEI). After that, the cells were opened in order to evacuate any possible gaseous product developed during SEI formation, sealed again and brought out of the box for characterization.

All the electrochemical measurements have been performed using a VMP2/Z galvanostat–potentiostat by PAR Instruments (Oak Ridge, TN).

Charge/discharge cycles were performed between 0.01 V and 1.5 V vs. Li^+/Li at C/5 (approximately 0.15 mA cm^{-2}) in the temperature range of 20 °C to −30 °C. The temperature was regulated within ±1 °C using a modified programmable freezer equipped with a vent for air circulation. The EIS spectra have been recorded in the frequency range of 1 mHz to 100 kHz with a 5 mV sinusoidal excitation over the selected bias potential.

Electrode morphologies were studied by SEM using a Cambridge Stereoscan mod. 369 electron microscope. X-ray photoelectron spectroscopy (XPS) measurements were performed using an Al Kα un-monochromatized source (1486.7 eV) at a base pressure of 10^{-9} Torr. The photoelectrons were analyzed with a CHA analyzer operating at a pass-energy of 58 eV. Ultraviolet photoelectron spectroscopy (UPS) measurements were performed in ultra high vacuum (10^{-9} Torr) with a He discharge lamp (40.8 eV). Electrons were collected with a CHA analyzer at a pass-energy of 2.9 eV.

3. Results

3.1. Structure and morphology

The electrode morphologies have been examined by scanning electron microscopy (SEM). The micrographs of electrodes containing Cu powders (Fig. 1a) show the same morphology of pristine partially oxidized graphite electrodes (see Ref. [25]), with graphite average particle size of the order of about 2 μm. Backscattered electron analysis reveals a quite uniform Cu dispersion in the case of graphite/Cu powder composite (Fig. 1b). Micrographs of Cu covered electrodes, showing a quite uniform deposit without evident macroscopic holes, may be found in Ref. [25].

X-ray photoelectron spectroscopy analysis of the electrodes, performed at energies near the Cu 2p binding energy (Fig. 2a), shows that most of the Cu present in the electrodes is in the metallic state (binding energy 932.8 eV). Deconvolution of the spectra reveals that only a minimal amount of metal is oxidized (Cu^{2+}, binding energy 935.2 eV). UPS analysis performed in the energy range near graphite valence bands (Fig. 2b) shows no differences in the shape of the spectra caused by the presence of Cu metal particles or layer. This means that the metal does not affect the graphite electronic levels. This result is not surprising, especially if one considers the very low amounts of metal involved (1% w/o for the electrodes containing dispersed Cu powder, and less than 1% for the electrodes coated with Cu layer).

3.2. Cyclic voltammetry (CV)

Slow-scan-rate CV has been utilized in order to determine the effects of the Cu metal coating and Cu powder addition on the intercalation mechanism and kinetics. Fig. 3 shows typical steady state cyclic voltammograms obtained at the scan rate of 10 μV s^{-1} in the potential range of 0.005–0.3 V vs. Li^+/Li at 20 °C for all electrodes. For comparison purposes, the curves have been normalized to the weight of the active material.

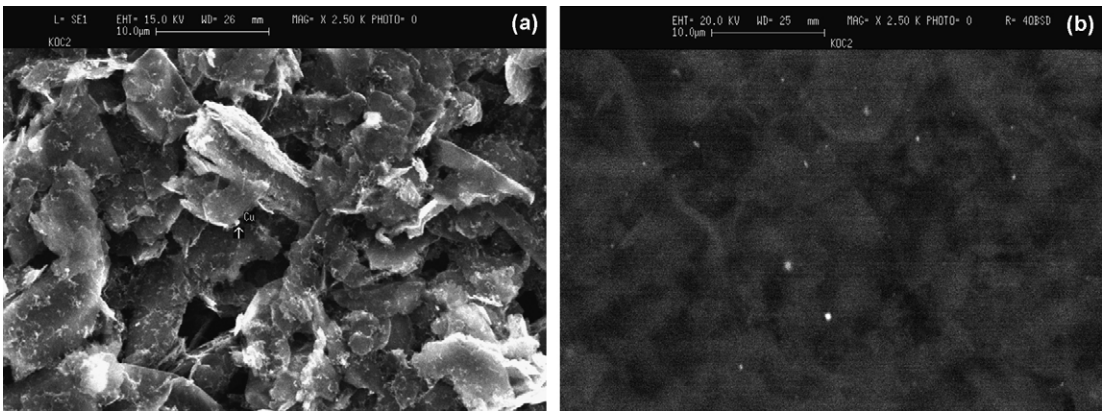

Fig. 1. Secondary electrons (a) and backscattered electrons (b) images for Cu-powder/graphite electrode.

At this low scan rate, the cyclic voltammograms are equivalent to a coulometry. The values of intercalated charge for all electrodes are close to the theoretical one of 372 mAh g^{-1} expected for natural graphite. This indicates that the modifications introduced by the Cu metal deposit and by the Cu powder dispersion do not appreciably affect the intercalation ability of the electrodes at room temperature.

The general shape of the cyclic voltammograms is the one expected for the natural graphite. Moreover, the mid-point potentials between the anodic and cathodic peaks of the three main processes, related to the three couples LiC_6/LiC_{12}, LiC_{12}/LiC_{27}, LiC_{36}/LiC_{72}, are very close to the reversible potentials (85 mV, 120 mV, and 210 mV, respectively) reported in the literature for natural graphite [35,36]. Peak shape and definition are an indication of the kinetics of the electrochemical processes. With this in mind, the comparison of the voltammograms of the pristine graphite with those of the modified electrodes leads to the conclusion that, in general, the addition of the metal powder to the bulk and/or the presence of a surface layer improve the peak definition and sharpness and thus the interfacial properties.

The comparison of the voltammograms of electrodes B and C demonstrates that the surface layer is more effective than the powder addition in decreasing the overall polarization. This may be deduced from intercalation/deintercalation peaks potentials that, especially for the couples LiC_6/LiC_{12}, LiC_{12}/LiC_{27}, are less negative

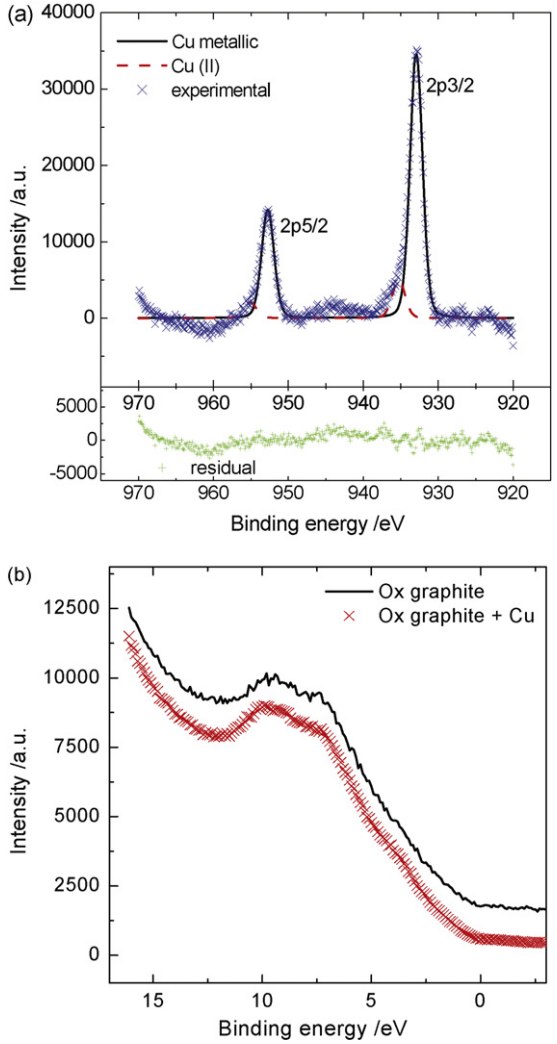

Fig. 2. Photoelectron spectra acquired near Cu 2p electrons energy (a) and near graphite valence bands energy (b).

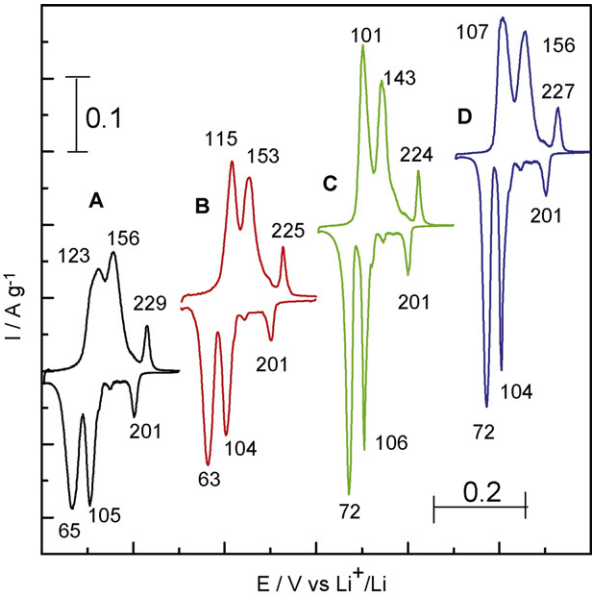

Fig. 3. Slow-scan-rate cyclic voltammograms for the electrodes A (oxidized graphite electrode), B (Cu powder/oxidized graphite composite), C (Cu layer/oxidized graphite composite), and D (Cu powder and layer/oxidized graphite composite). For sake of clarity, all the curves are shifted along both axes.

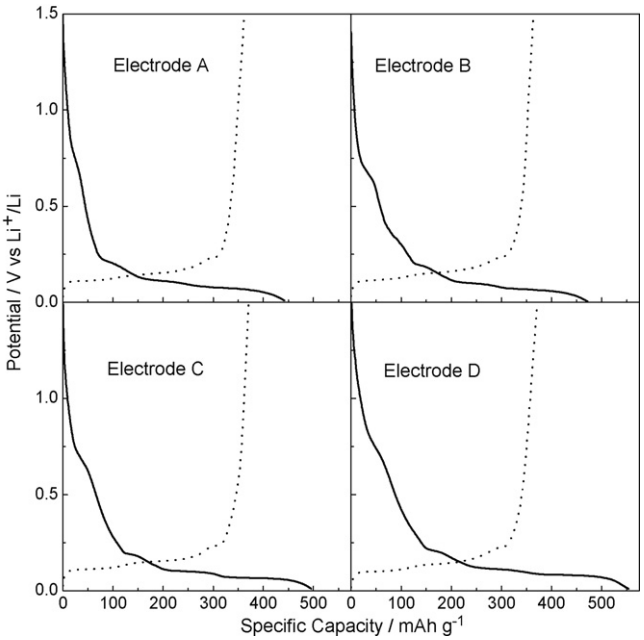

Fig. 4. Galvanostatic intercalation (—) and deintercalation (···) profiles of the 1st cycle. C/3 rate, $T = 20\,^{\circ}C$.

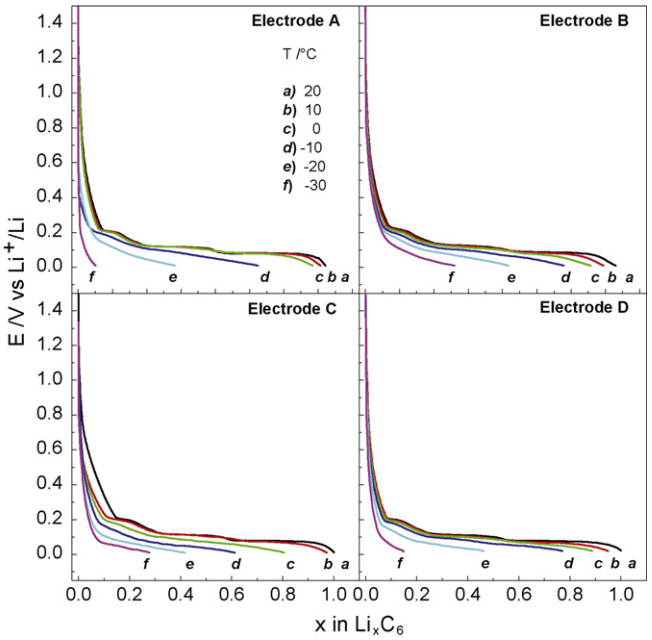

Fig. 5. Galvanostatic intercalation profiles at different temperatures obtained at C/5 rate after complete deintercalation at $T = 20\,^{\circ}C$.

and less positive, respectively, for electrode C than for electrode B.

For electrodes C and D only the deintercalation curves seem to be affected with a greater polarization for electrode D than for electrode C.

3.3. Galvanostatic measurements

The cycling stability at C/5 rate of type A, B and C electrodes at room temperature has been reported elsewhere [4,25]. All electrodes are stable upon continuous cycling with capacities close to the theoretical value of natural graphite. The same results have been obtained for electrode D.

Fig. 4 shows the first intercalation and deintercalation profiles recorded at room temperature and C/3 rate for the different electrodes. In addition to the reversible lithium–graphite staging plateaus, the expected extra feature due to the irreversible SEI build-up is present at about 0.8 V. The lowest irreversible capacity, computed as the difference between first intercalation and first deintercalation capacity (see also Table 1) is the one of the pristine electrode. Among the Cu modified electrodes the irreversible capacity increases in going from electrodes B, C and D. These results suggest that the SEI formation on the Cu-modified electrodes follows different paths with respect to the pristine graphite and, as the highest value is found for the electrode D, that the contributions introduced by dispersed powder and layered metal toward SEI formation are additive.

Fig. 5 shows the reversible intercalation profile obtained at C/5 rate and at different temperatures for each kind of electrode. The curves relative to electrodes A and B are reproduced from Ref. [4] and inserted for sake of comparison. The curves and the reversible capacity data (average of five different cycles) listed in Table 1 have been obtained by cycling the electrodes at the selected temperature after a complete deintercalation step at room temperature. This means that the starting conditions are the same for all curves and, consequently, that the capacity values refer to the true intercalation capacity at each temperature, free from eventual bias due to the previous history. Apart from eventual effect of aging, the responses depend only on the kinetics of the electrochemical intercalation reaction. From the listed values and from the curves it may be inferred that all the electrodes have a similar electrochemical behavior down to $-20\,^{\circ}C$. At $-30\,^{\circ}C$ the composite electrode containing Cu powder has the highest intercalation capacity with a final limiting composition of about $Li_{0.33}C_6$. The other Cu modified electrodes behave better than the pristine partially oxidized graphite but the limiting capacity is about one half of that of the Cu-powder containing electrode.

3.4. Electrochemical impedance spectroscopy (EIS)

Impedance spectra at different temperatures in the range from $20\,^{\circ}C$ to $-30\,^{\circ}C$ have been collected at selected potentials between 250 mV and 50 mV starting from the more positive potential. The electrodes were first equilibrated at the selected bias potential for at

Table 1
Values of specific intercalation capacity as obtained by intercalating at various temperatures electrodes previously fully deintercalated at $20\,^{\circ}C$ (see text for further details).

Electrode		Irrev.[a]	Reversible					
		20 °C	20 °C	10 °C	0 °C	−10 °C	−20 °C	−30 °C
A	Ox[b]	84	364	361	361	260	201	26
B	Ox + Cu 1%[b]	111	364	346	327	290	208	130
C	Ox + Cu 50 Å	126	372	361	310	294	156	103
D	Ox + Cu 1% + Cu 50 Å	190	372	353	335	280	175	60

[a] C/3 rate.
[b] From Ref. [4].

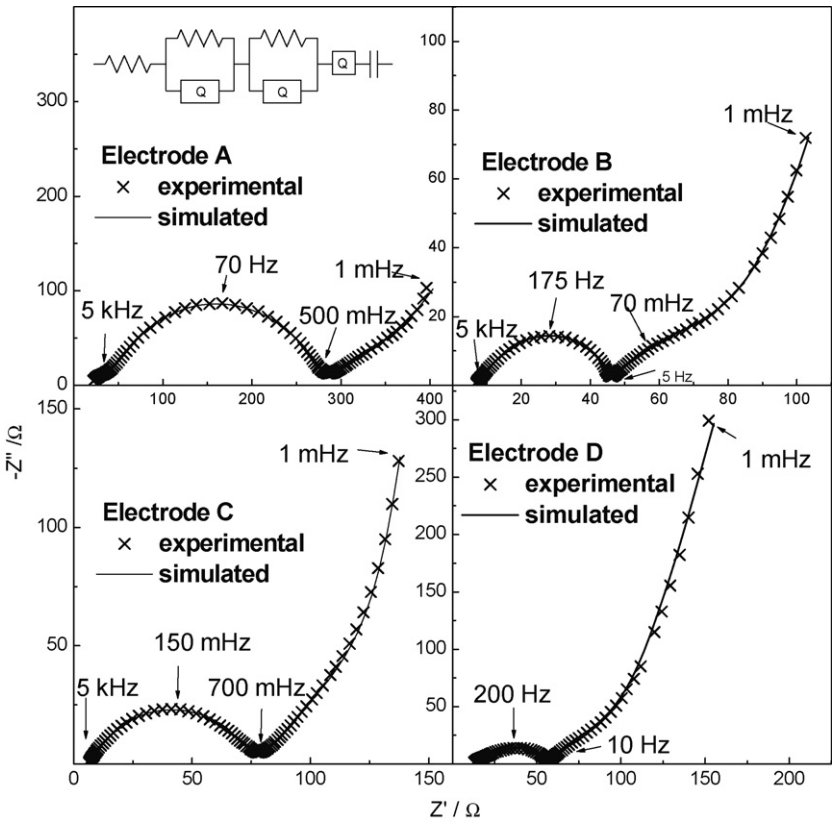

Fig. 6. Experimental (×) and simulated (—) Nyquist plots obtained at $E = 0.1$ V and $T = 20\,^{\circ}$C. The insert shows the equivalent circuit used to fit the spectra.

least 5 h at room temperature. Spectra were subsequently recorded at each temperature starting from the higher one after at least 5 h equilibration at constant potential and temperature. This procedure assures that the state of charge for each set of impedance measurements is the same at any temperature. Representative dispersions for the different electrodes at 0.1 V and 20 °C are shown in Fig. 6. The impedance dispersions are directly comparable as the graphite loadings are very close and the electrode geometries are the same. In these conditions the mass ratios can be used as scaling factor [36,37]. All the impedance dispersions show common features from high to low frequencies: namely, two overlapped depressed semicircles in the high- and middle-frequency region, describing the accumulation of charge at the surface of passivation layer and the charge transfer process and a low-frequency region in which a 45° dispersion bends toward a vertical line, describing a diffusion to a blocking electrode. The middle frequency semicircle, associated with the charge transfer process is the dominant feature of the spectra.

As detailed in Ref. [25] at some potentials the diffusion process of the graphite electrodes modified with a surface layer, either Cu or Sn, is not described by an ideal 45° Warburg-like line, but an inflection is present in the middle-to-low-frequency region of the spectra. This holds also for the spectra of electrodes B and D and may be ascribed to deviations of the diffusion conditions from ideal behavior [38–41] caused by heterogeneities of the electrode composition or thickness leading to the existence of several microscopic diffusion processes [42–44] having different characteristic diffusion times. This causes the appearance in the dispersion of a distributed element deviating from the 45° Warburg straight line. The same type of deviations have also been found in the spectra of mesoporous carbon electrodes [45,46], where Li^+ solid-state diffusion through the planes of the active graphite and Li^+ diffusion in the liquid trapped inside the mesopores are relevant.

The most important property revealed by EIS spectra of Cu–graphite composites B, C and D is, however, the decrease of the overall impedance in comparison with the pristine electrode A. This behavior is retained when the temperature is lowered as shown in Fig. 7 for the electrodes A and B. Electrodes C and D exhibit a similar behavior. The middle-frequency semicircle associated with the charge transfer resistance is, for all electrodes, the main factor that causes the increase of the overall impedance as the temperature is lowered.

The experimental impedance data have been analyzed by fitting the dispersions to an equivalent circuit commonly used to describe an intercalation process complicated by a slow interfacial charge transfer [25–31]. In Boukamp's notation [47] the equivalent circuit may be written as: $R_{el}(R_{sei}C_{sei})(R_{ct}C_{dl})WC_i$. R_{el}, R_{sei} and R_{ct} describe the resistances associated with the solution, the passivation layer and charge transfer process, respectively. C_{sei} and C_{dl} are the capacities associated with the passivation layer and double layer, respectively. W and C_i describe the diffusion to a blocking electrode and the intercalation capacity. During the simulation all the capacities and the Warburg diffusion element have been substituted with the constant phase element Q that better describes deviations of the electrode from ideality. The circuit is schematized in the insert of Fig. 6. In the same figure the line and the points represent the simulated spectra and experimental points, respectively. As it may be seen the agreement between the experimental data and the simulated spectra is rather good. In some cases, especially at low temperatures, it has been difficult to separate the contribution of the SEI from the charge transfer semicircle. In spite of

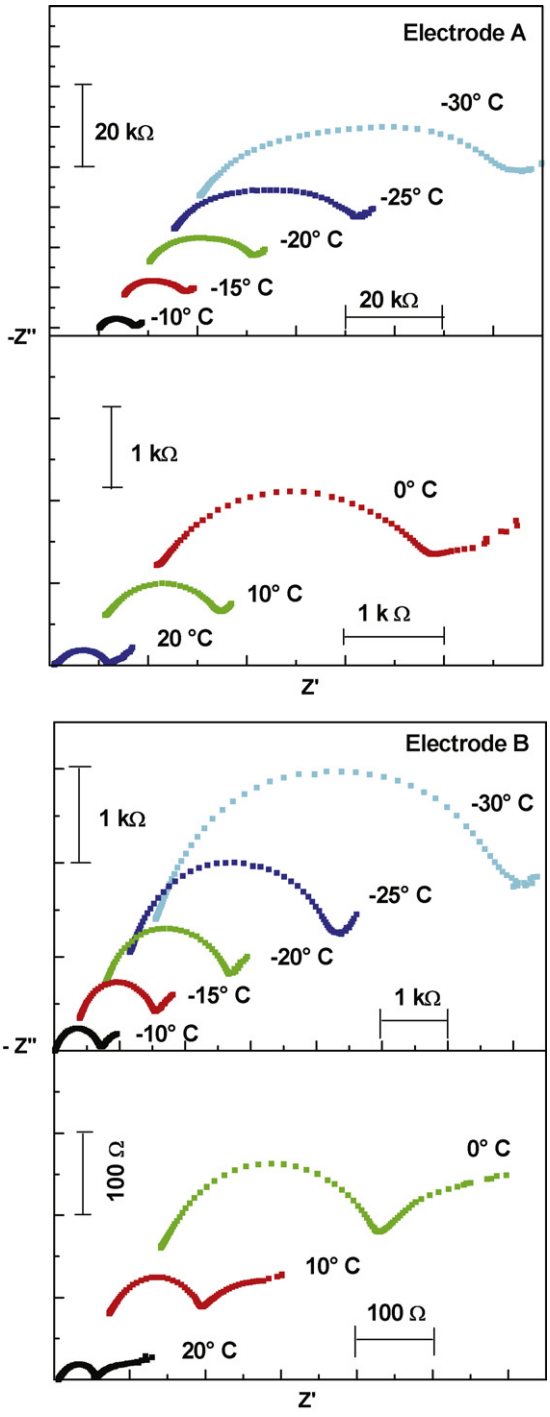

Fig. 7. Nyquist plots for electrodes A and B at different temperatures and 90 mV vs. Li^+/Li bias potential.

this, χ^2 values of the order of $10^{-4}/10^{-5}$ have been obtained in all cases.

The computed SEI resistances as a function of the temperature are plotted in Fig. 8. The plotted points are the average of the values obtained at the different potentials. The large error bars reflect the difficulties found in separating the high frequency from the middle frequency semicircles. In spite of this some general considerations may be drawn from the trend of the plotted values. The SEI resistance of the composite electrodes B, C and D is lower than that of the pristine electrode A over the whole temperature range. The temperature variation is greater for the pristine and for electrode D

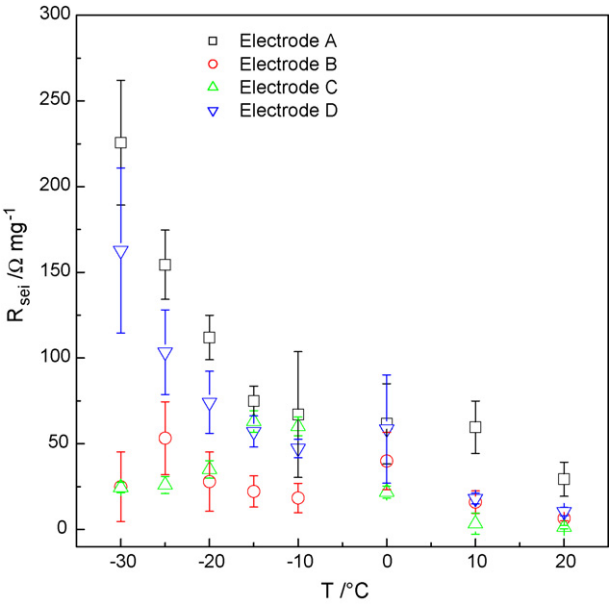

Fig. 8. Average values of R_{sei} at different temperatures.

containing Cu both as powder and layer. Lower values and temperature dependence of SEI resistance are found for electrodes B and C. These observations, together with the trend of the irreversible capacity values, suggest that SEI chemistry is quite different in the pristine and composite electrodes. However, additional studies are needed to draw definitive conclusions.

The calculated values of R_{ct} of all the electrodes at different potentials and at some relevant temperatures (20 °C, 0 °C, and −30 °C) are shown in Fig. 9. In this case the errors in the simulation are much lower than in the case of the SEI resistance simply because the relative semicircle is the dominant feature of the spectra and accounts for most of the impedance. As it may be seen, at any temperature and potential the charge transfer resistances of the Cu modified electrodes are lower than those of the pristine oxidized graphite electrode.

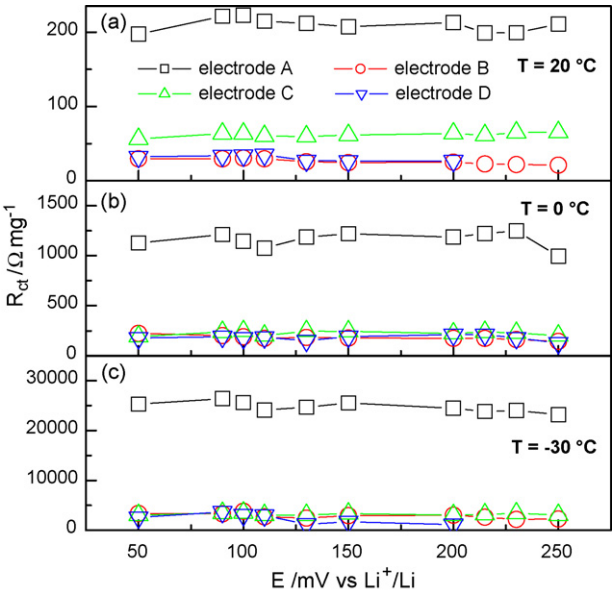

Fig. 9. Fitted values of R_{ct} or electrodes A, B, C and D vs. bias potential at: (a) 20 °C; (b) 0 °C; (c) −30 °C.

It has been recently recognized [26–30] that the so-called "charge transfer resistance" in graphite intercalation electrodes is largely associated with the rate of desolvation of Li^+ ions at the electrode solution interface: i.e. the so-called "adatom model" [48]. Adsorption and desolvation precede Li^+ intercalation into graphite and the concomitant electron transfer from the current collector to the host network to restore electroneutrality [25,48]. A similar model has also been applied to oxide cathodes [49–51]. As a consequence the intercalation rate does not follow a Butler–Volmer type relationship with electrode potential, but depends only on the energy related to adsorption and desolvation processes [48]. The model can be applied also in the present case as the R_{ct} values, at any temperature, are practically constant over the potential range of 50–250 mV.

The decreased charge transfer resistance, and hence the improved charge transfer kinetics, caused by the presence of the metal may be probably explained by assuming that the metal acts as a sort of catalyst for the desolvation reaction.

This interpretation of Cu role is in agreement with Huang et al. [31] that suggest a catalytic effect of some transition metals, either as oxides or in metallic state, on the intercalation of Li^+ into graphite through a mechanism that involves an enhancement of the desolvation rate and an increase of electronic density at the surface of the electrode/electrolyte interface.

By assuming that the charge transfer resistance is a simple thermally activated process [26–30] the reciprocal of the computed R_{ct} values have been fitted to the Arrhenius type equation

$$\frac{1}{R_{ct}} = A_0\ e^{-E_a/RT} \quad (1)$$

where A_0, R and E_a are a pre-exponential factor, the gas constant and the activation energy, respectively. The plots for electrodes A and C are shown in Fig. 10. Each line is relative to a different potential as listed in the figure. Similar plots, not shown for sake of brevity, have been obtained for the other electrodes. The average values of the activation, energies are 57.1 ± 2.3 kJ mol^{-1}, 51.1 ± 1.3 kJ mol^{-1}, 49.8 ± 1.4 kJ mol^{-1} and 49.4 ± 3.4 kJ mol^{-1} for electrodes A, B, C and D, respectively. The values are consistent with those reported by Xu et al. [30] who correlated the charge transfer resistance and the energy required to break-up of the lithium solvation shell at the graphite/electrolyte interface with the solvent (EC, DEC, DMC and their mixtures) composition and the type and concentration of the supporting electrolyte salts ($LiClO_4$, $LiPF_6$, and $LiBF_4$) as well as with the chemistry of the SEI.

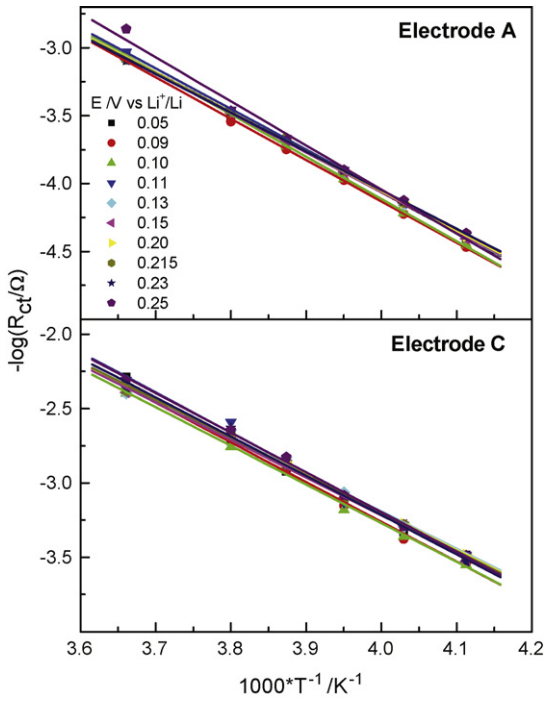

Fig. 10. Arrhenius plots of the reciprocal of the computed charge transfer resistance.

4. Discussion

The lower values of the activation energies for the electrodes containing copper with respect to the pristine electrode testify an active role of the metal in decreasing the energy barrier for the desolvation reaction, and justify the lower charge transfer resistances. The activation energy values for the electrodes C and D are slightly lower than those found for the electrode B. This reflects the better kinetics observed in the cyclic voltammograms of electrodes C and D with respect to the electrode B and suggests that the catalytic effect of the Cu is more effective when the metal is present as a surface layer than as a dispersed powder in the electrode bulk.

However, as seen from Table 1, the reversible capacity at the lower temperatures are higher for electrode B than for electrodes C and D. Hence, the addition of Cu powder appears to be more effective than a surface layer in improving low-temperature performances. In this case the metal probably produces a bulk effect by improving the conductivity and decreasing the SEI resistance. An alternative and additional possible explanation of the lower intercalation capacity at low temperature of the metal covered electrodes may be related to the mechanism of mass transfer through the copper layer. This is believed [19] to occur in the vacant space not occupied by copper ions in the metal lattice during lattice vibrations whose amplitude obviously decrease with decreasing temperature.

These considerations, together with the behavior of electrode D that is both bulk and surface modified, and displays, among the modified electrodes, the lowest intercalation ability at −30 °C and R_{ct} values comparable with those of electrodes B and C, still leave some open questions about the interaction of the two modifications, even if a generalized performance improvement of all the Cu–graphite composites in comparison with the pristine graphite electrode is confirmed.

5. Conclusions

Cu/graphite composites showed an improvement in the Li intercalation ability at low temperature. Electrochemical impedance spectroscopy has been utilized in order to explain the reasons for the reduced polarization and for the improved performances. It has been shown that the main effect consists in a reduction of the charge transfer resistance, probably due to the catalytic role of Cu either as dispersed powders or as a thin film cover, overall the entire temperature range investigated.

Further investigations are currently in progress in order to evaluate the interactions with other electrolytes and the behavior of electrodes containing other metals, particularly those able to form alloys with Li, in order to study the type of mechanism operative at the level of lithium transfer through the interface and the changes in the SEI chemistry induced by the metal.

Acknowledgement

This work was supported by MIUR, PRIN 2007.

References

[1] C.K. Huang, J.S. Sakamoto, J. Wolfenstine, S. Surampudi, J. Electrochem. Soc. 147 (2000) 2893.
[2] S.S. Zhang, K. Xu, T.R. Jow, Electrochim. Acta 48 (2002) 241.
[3] H.P. Lin, D. Chua, M. Salomon, H.C. Shiao, M. Hendrickson, E. Plichta, S. Slane, Electrochem. Solid-State Lett. 4 (2001) A71.
[4] F. Nobili, S. Dsoke, T. Mecozzi, R. Marassi, Electrochim. Acta 51 (2005) 536.
[5] E. Peled, C. Menachem, D-Bar-Tow, A. Melman, J. Electrochem. Soc. 143 (1996) L4.
[6] C. Menachem, E. Peled, L. Burstein, Y. Rosenberg, J. Power Sources 68 (1997) 277.
[7] C. Menachem, Y. Wang, J. Flowers, E. Peled, S.G. Greenbaum, J. Power Sources 76 (1998) 180.
[8] R.S. Rubino, E.S. Takeuchi, J. Power Sources 81–82 (1999) 373.
[9] S.S. Zhang, K. Xu, T.R. Jow, J. Solid State Electrochem. 7 (2003) 147.
[10] S.S. Zhang, K. Xu, T.R. Jow, Electrochem. Commun. 4 (2002) 928.
[11] E.J. Plichta, M. Hendrickson, R. Thompson, G. Au, W.K. Behl, M.C. Smart, B.V. Ratnakumar, S. Surampudi, J. Power Sources 94 (2001) 160.
[12] M.C. Smart, B.V. Ratnakumar, S. Surampudi, J. Electrochem. Soc. 149 (2002) A361.
[13] T. Takamura, J. Suzuki, C. Yamada, K. Sumiya, K. Sekine, Surf. Eng. 15 (1999) 225.
[14] T. Takamura, K. Sumiya, J. Suzuki, C. Yamada, K. Sekine, J. Power Sources 81–82 (1999) 368.
[15] P. Yu, J.A. Ritter, R.E. White, B.N. Popov, J. Electrochem. Soc. 147 (2000) 2081.
[16] J.Y. Lee, R. Zhang, Z. Liu, J. Power Sources 90 (2000) 70.
[17] P. Yu, J.A. Ritter, R.E. White, B.N. Popov, J. Electrochem. Soc. 147 (2000) 1280.
[18] B. Veeraraghavan, A. Duraviajan, B. Haran, B. Popov, R. Guidotti, J. Electrochem. Soc. 149 (2002) A675.
[19] J. Suzuki, M. Yoshida, C. Nakahara, K. Sekine, M. Kikuchi, T. Takamura, Electrochem. Solid-State Lett. 4 (1) (2001) A1.
[20] V.G. Khomenko, V.Z. Barsukov, J.E. Doninger, I.V. Barsukov, J. Power Sources 165 (2007) 598.
[21] N.L. Rock, P.N. Kumta, J. Power Sources 164 (2007) 829.
[22] M. Yoshio, T. Tsumura, N. Dimov, J. Power Sources 163 (2006) 215.
[23] G.X. Wang, J.H. Ahn, J. Yao, S. Bewlay, H.K. Liu, Electrochem. Commun. 6 (2004) 689.
[24] B.-C. Kim, H. Uono, T. Satou, T. Fuse, T. Ishihara, M. Ue, M. Senna, J. Electrochem. Soc. 152 (2005) A523.
[25] F. Nobili, S. Dsoke, M. Mancini, R. Tossici, R. Marassi, J. Power Sources 180 (2008) 845.
[26] K. Xu, J. Electrochem. Soc. 154 (2007) A162.
[27] A. Funabiki, M. Inaba, T. Abe, Z. Ogumi, J. Electrochem. Soc. 146 (1999) 2443.
[28] T. Abe, H. Fukuda, Y. Iriyama, Z. Ogumi, J. Electrochem. Soc. 151 (2004) A1120.
[29] T. Abe, Y. Mizutami, N. Kawabata, M. Inaba, Z. Ogumi, Synth. Met. 125 (2002) 249.
[30] K. Xu, Y. Lam, S.S. Zhang, T.R. Jow, T.B. Curtis, J. Phys. Chem. C 111 (2007) 7411.
[31] H. Huang, E. M: Kelder, J. Schonman, J. Power Sources 97–98 (2001) 114.
[32] M.C. Smart, B.V. Ratnakumar, S. Surampudi, J. Electrochem. Soc. 146 (1999) 486.
[33] H.C. Shiao, D. Chua, H.P. Ling, S. Slane, M. Salomon, J. Power Sources 87 (2000) 167.
[35] T. Ohzuku, Y. Iwakoshi, K. Sawai, J. Electrochem. Soc. 140 (1993) 2490.
[36] M.D. Levi, D. Aurbach, J. Electroanal. Chem. 421 (1997) 79.
[37] M.D. Levi, D. Aurbach, J. Phys. Chem. B 101 (1997) 4641.
[38] D. Aurbach, M. Levi, E. Levi, H. Teller, B. Markovsky, G. Salitra, U. Heider, L. Heider, J. Electrochem. Soc. 145 (1998) 3024.
[39] J.P. Meyers, M. Doyle, R.M. Darling, J. Newman, J. Electrochem. Soc. 147 (2000) 2930.
[40] M.D. Levi, D. Aurbach, J. Phys. Chem. B 108 (2004) 11693.
[41] M.D. Levi, D. Aurbach, J. Phys. Chem. B 101 (1997) 4630.
[42] E. Barsoukov, J. Ross Macdonald, Impedance Spectroscopy. Theory, Experiments and Applications, second edition, John Wiley & Sons, New York, 2005, p. 83.
[43] E. Barsoukov, J. Ross Macdonald, Impedance Spectroscopy. Theory, Experiments and Applications, second edition, John Wiley & Sons, New York, 2005, p. 445.
[44] E. Barsoukov, J. Ross Macdonald, Impedance Spectroscopy. Theory, Experiments and Applications, second edition, John Wiley & Sons, New York, 2005, p. 457.
[45] E. Barsoukov, J. Hyun Kim, J. Hun Kim, C.O. Yoon, H. Leem, Solid State Ionics 116 (1999) 249.
[46] Y.-C. Chang, H.-J. Sohn, J. Electrochem. Soc. 147 (2000) 50.
[47] B.A. Boukamp, Solid State Ionics 20 (1986) 159.
[48] P.G. Bruce, M.Y. Saidi, J. Electroanal. Chem. 322 (1992) 93.
[49] F. Croce, F. Nobili, A. Deptula, W. Lada, R. Tossici, A. D'Epifanio, B. Scrosati, R. Marassi, Electrochem. Commun. 1 (1999) 605.
[50] F. Nobili, R. Tossici, F. Croce, B. Scrosati, R. Marassi, J. Power Sources 94 (2001) 238.
[51] F. Nobili, R. Tossici, R. Marassi, F. Croce, B. Scrosati, J. Phys. Chem. B 106 (2002) 3909.